

Ethane-Bridged Organosilica Nanotubes Functionalized with Arenesulfonic Acid and Phenyl Groups for the Efficient Conversion of Levulinic Acid or Furfuryl Alcohol to Ethyl Levulinate

Daiyu Song,^[b] Sai An,^[b] Yingnan Sun,^[a] Panpan Zhang,^[a] Yihang Guo,^{*,[a]} and Dandan Zhou^{*,[a]}

A series of ethane-bridged organosilica nanotubes functionalized with arenesulfonic acid and phenyl groups (ArSO₃H-Si(Et)Si-Ph-NTs) was fabricated successfully by a P123-directed sol-gel co-condensation route combined with hydrothermal treatment with a carefully adjusted P123-to-bis-silylated organic precursor-to-HCl molar ratio in the starting system. The morphological characteristics, textural properties, Brønsted acidity, surface hydrophobicity, and structural integrity of the carbon/

silica framework were characterized. The ArSO₃H-Si(Et)Si-Ph-NTs materials were applied in the synthesis of ethyl levulinate from the esterification of levulinic acid and the ethanolysis of furfuryl alcohol, and the excellent catalytic activity was explained in terms of the strong Brønsted acidity, unique hollow nanotube morphology, and enhanced surface hydrophobicity. Reusability tests confirmed that ArSO₃H-Si(Et)Si-Ph-NTs can be reused for three or five times without a significant loss of activity.

Introduction

Abundant and renewable biomass is regarded as a promising alternative to non-renewable resources for the production of sustainable biofuels and biochemicals as a result of the deterioration of the environment and the inevitable depletion of fossil resources. The development of new technologies to produce liquid fuels and value-added chemicals from the conversion of biomass has become an important research field in green chemistry.^[1–4] Among these explorations, the synthesis of alkyl levulinates from biomass-derived platform molecules such as levulinic acid or furfuryl alcohol is one of the most popular research topics. Alkyl levulinates, which include methyl, ethyl, and *n*-butyl levulinate, have found extensive applications in the flavoring and fragrance industries and as precursors to produce chemicals (e.g., γ -valerolactone) that can be converted into liquid alkanes and transportation fuels.^[5–7] Alkyl levulinates can be obtained in good yields through different routes such as the direct esterification of levulinic acid with alcohols and the alcoholysis of furfuryl alcohol under acid catalysis. A variety of homogeneous catalysts, such as sulfuric acid, hydrofluoric acid, and *p*-toluenesulfonic acid, have been

used for the synthesis of alkyl levulinates, however, they suffer from drawbacks such as corrosion, pollution, complex downstream neutralization, and difficult separation.^[8–10] Therefore, the use of heterogeneous acid catalysts has attracted much attention as such environmentally friendly approaches are easy to work up for the biomass-conversion processes. However, the reported heterogeneous acid catalysts, such as macroporous ion-exchange resins (e.g., Amberlyst-15),^[11,12] microporous zeolites (e.g., HZSM-5),^[13,14] mesoporous aluminosilicates (e.g., Al-TUD-1),^[15] sulfated metal oxides (e.g., SO₄²⁻/TiO₂ and SO₄²⁻/ZrO₂),^[12] and sulfonic acid grafted silica (e.g., SO₃H-SBA-15),^[13,16] have been thus far unsatisfactory for the esterification of levulinic acid and the alcoholysis of furfuryl alcohol because of the low densities or poor accessibility of the acid sites, easy deactivation, and low thermal stability.

Recently, inorganic mesoporous silica or periodic mesoporous organosilica (PMO) materials functionalized with organosulfonic acid have attracted particular attention in a variety of acid-catalyzed reactions and they are alternatives to hazardous homogeneous acids because of their advantages that include strong Brønsted acid properties, plentiful acid sites, high hydrothermal stability, and ease of separation.^[17–24] However, their long pore channels may lead to an increased diffusion distance for the reactants and products, which limit their catalytic activity to some extent because of the insufficient accessibility of the acid sites. To further improve the catalytic activity of organosulfonic acid functionalized silica materials in environmental friendly biomass-transformation processes such as esterification, transesterification, or ethanolysis, the morphology-controlled preparation of organosulfonic acid functionalized organosilica nanohybrids with 1D tubular (e.g., arenesulfonic

[a] Y. Sun, P. Zhang, Prof. Dr. Y. Guo, Prof. Dr. D. Zhou
School of Environment
Northeast Normal University
Changchun 130117 (PR China)
Fax: (+86)431-89165626
E-mail: guoyh@nenu.edu.cn

[b] D. Song, S. An
School of Chemistry
Northeast Normal University
Changchun 130024 (PR China)

Supporting information for this article can be found under <http://dx.doi.org/10.1002/cctc.201600083>.

or propylsulfonic functionalized ethane- or benzene-bridged organosilica nanotubes; Si(Ph/Et)Si-Ar/Pr-SO₃H NTs^[25] and 3D hollow spherical nanostructures (Pr/ArSO₃H-Et/Ph-HNS^[21]) were realized. The tubular or spherical SO₃H-based organosilica nanohybrids with advantages that include short diffusion and mass-transfer pathways, thin walls or shell thickness (several nanometers), and unique textural properties resulted in the increased accessibility of the guest molecules to the acid sites, and thereby, a much higher acid catalytic activity with respect to their bulk mesoporous counterparts was obtained.^[21,25,26]

Nevertheless, the surface hydrophilicity/hydrophobicity of solid acids has an influence on the catalytic activity and reusability in the synthesis of alkyl levulinates by esterification or ethanolysis.^[27] For the esterification of levulinic acid, the by-product of water can decrease the formation rate of alkyl levulinates. Although furfuryl alcohol can be used effectively for the synthesis of alkyl levulinates by acid-catalyzed alcoholysis, oligomeric byproducts were generated inevitably. These byproducts adsorbed on the surface of solid acid catalysts to lead to the low accessibility of the acid sites and poor reusability.^[28] These problems are expected to be alleviated by increasing the surface hydrophobicity of the solid acids.

In this work, a series of ethane-bridged organosilica nanotubes functionalized with arenesulfonic acid and phenyl groups (ArSO₃H-Si(Et)Si-Ph-NTs) were fabricated successfully by a P123-directed sol-gel co-condensation route combined with hydrothermal treatment. Compared with our previously reported Pr/ArSO₃H-Et/Ph-HNS that contained one type of hydrophobic moiety (bridging ethyl groups), the introduction of the second hydrophobic moiety, that is, terminal phenyl groups, into the silica/carbon framework of the organic-inorganic hybrid silica materials can further improve the surface hydrophobicity of the nanohybrids. Accordingly, the adsorption of hydrophilic byproducts that occurred in the esterification or ethanolysis process on the adjacent organosulfonic acid groups can be further inhibited, and an enhanced catalytic activity and stability of the esterification and ethanolysis reactions are expected.

To evaluate the heterogeneous acid catalytic performance of the ArSO₃H-Si(Et)Si-Ph-NTs, the esterification of levulinic acid with ethanol and the ethanolysis of furfuryl alcohol were se-

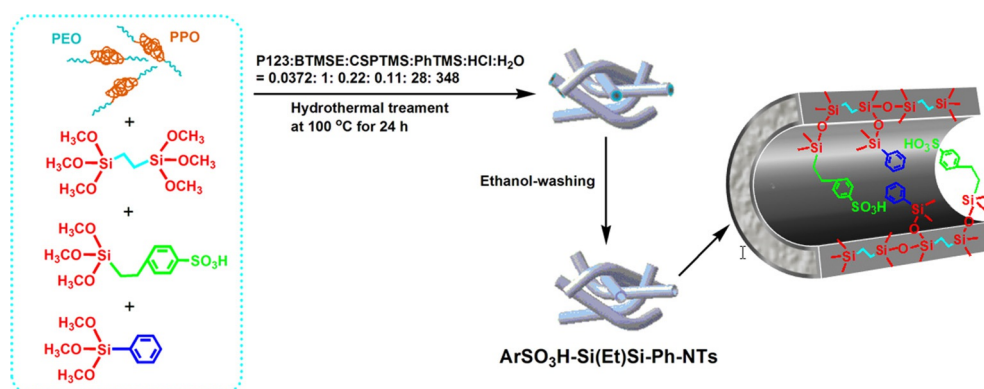
lected as the model reactions. For comparison, arenesulfonic or propylsulfonic acid functionalized ethane-bridged organosilica nanotubes, ArSO₃H-Si(Et)Si-NTs and PrSO₃H-Si(Et)Si-NTs, respectively, ordered mesoporous propylsulfonic acid functionalized SBA-15 silica, a commercially available sulfonic ion-exchange resin (Amberlyst-15), and H₂SO₄ were also tested under the same conditions. As a result of the combination of advantages that include strong Brønsted acidity, unique hollow tubular nanostructure, excellent porosity properties, and enhanced hydrophobicity at the surface, the as-prepared functionalized ArSO₃H-Si(Et)Si-Ph-NTs nanohybrids are expected to exhibit excellent heterogeneous acid catalytic activity and stability in the synthesis of ethyl levulinate from biomass-derived platform molecules.

Results and Discussion

Catalyst preparation

P123-directed sol-gel co-condensation combined with hydrothermal treatment was applied to fabricate 1D hollow tubular ArSO₃H-Si(Et)Si-Ph-NTs materials. The preparation procedure included the cohydrolysis and co-condensation of the bis-silylated organic unit 1,2-bis(trimethoxysilyl)ethane (BTMSE; silica/carbon framework that contained organic building blocks to provide bridging ethane moieties for the nanohybrids), silylated organic unit phenyltrimethoxysilane (PhTMS; silica/carbon framework that contained organic building blocks to provide terminal phenyl moieties for the nanohybrids), and silylated organic unit 2-(4-chlorosulfonylphenyl)ethyl trimethoxysilane that contained arenesulfonic acid (CSPTMS; organic building block to provide acid sites for the nanohybrids) under acidic conditions (Scheme 1). This route is a better method to construct the organosulfonic acid functionalized organic-inorganic hybrid silica materials than the postsynthetic grafting method because of the advantages of the homogeneous dispersion of the acid sites and strong interaction between the acid sites with the silica/carbon framework.^[29,30]

P123 is an amphiphilic copolymer surfactant that contains both hydrophilic PEO [poly(ethylene oxide)] and hydrophobic PPO [poly(propylene oxide)] blocks, and it can readily self-as-



Scheme 1. Illustration of P123-templated preparation and wall structure of the functionalized ArSO₃H-Si(Et)Si-Ph-NTs nanohybrids.

semble into micelles through hydrogen bonding and hydrophobic/hydrophilic interactions under acidic conditions. The micelles can further aggregate to form lyotropic liquid crystal structures with various morphologies. Herein, to fabricate 1D hollow tubular $\text{ArSO}_3\text{H-Si(Et)Si-Ph}$ nanohybrids, the molar ratio of P123-to-BTMSE-to-HCl of 0.0372:1:28 in the starting preparation system was adjusted carefully. Under these conditions, a tubular lyotropic liquid crystal structure was created because of the suitable hydrolysis and condensation rate and surface hydrophilicity/hydrophobicity of BTMSE, which can prevent P123 micelles from aggregation. Moreover, the rigidity of BTMSE can stabilize the rodlike micelles. After hydrothermal treatment and subsequent washing with boiling ethanol, $\text{ArSO}_3\text{H-Si(Et)Si-Ph}$ nanotubes were fabricated (Figure 1 a–c). However, under the same molar ratio but with the replacement of BTMSE with the silylated inorganic unit tetraethyl orthosilicate (TEOS), highly ordered 2D mesostructured $\text{PrSO}_3\text{H-SBA-15}$ silica was constructed (Figure 1 f). In comparison to those of the BTMSE precursor, the hydrolysis and condensation rates of TEOS are faster; additionally, the surface hydrophilicity of TEOS is stronger, which can induce the cylindrical packing of P123 micelles for the formation of mesoporous $\text{PrSO}_3\text{H-SBA-15}$ nanoparticles.^[31]

Catalyst characterization

Morphologies, textural properties, and crystal phases

The morphologies, textural properties, and crystal phases of the as-prepared organosulfonic acid functionalized silica materials were characterized by using TEM (Figure 1) and N_2 porosimetry measurements (Figure 2).

$\text{ArSO}_3\text{H-Si(Et)Si-Ph-NTs}$ with various SO_3H loadings (4.8, 7.2, and 8.2 wt%) exhibit 1D hollow tubular nanostructures, and several $\text{ArSO}_3\text{H-Si(Et)Si-Ph}$ nanotubes twist together (Figure 1 a–c). The estimated inner diameter, outer diameter, and wall thickness of $\text{ArSO}_3\text{H-Si(Et)Si-Ph-NTs}$ are 5, 11, and 3 nm, respectively (Table 1). The organosulfonic acid functionalized ethane-bridged organosilica nanohybrids without phenyl groups, $\text{7.3ArSO}_3\text{H-Si(Et)Si-NTs}$ and $\text{6.8PrSO}_3\text{H-Si(Et)Si-NTs}$, exhibit a similar morphology to $\text{ArSO}_3\text{H-Si(Et)Si-Ph-NTs}$ (Figure 1 d

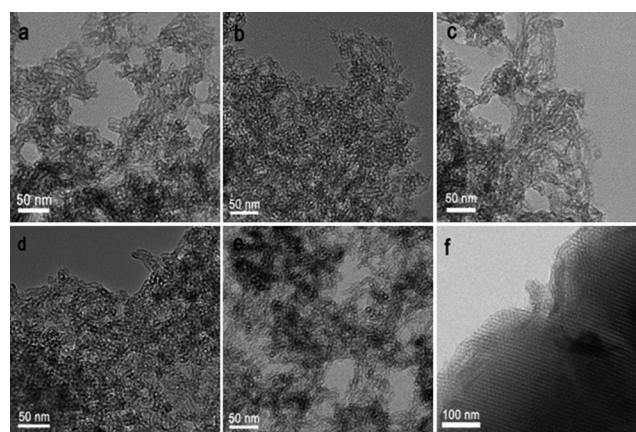


Figure 1. TEM images of a) $4.8\text{ArSO}_3\text{H-Si(Et)Si-Ph-NTs}$, b) $7.2\text{ArSO}_3\text{H-Si(Et)Si-Ph-NTs}$, c) $8.2\text{ArSO}_3\text{H-Si(Et)Si-Ph-NTs}$, d) $7.3\text{ArSO}_3\text{H-Si(Et)Si-NTs}$, e) $6.8\text{PrSO}_3\text{H-Si(Et)Si-NTs}$, and f) $6.7\text{PrSO}_3\text{H-SBA-15}$.

and e). $6.7\text{PrSO}_3\text{H-SBA-15}$ displays a long-range hexagonal arrangement of parallel pore channels (Figure 1 f) with a pore diameter of ≈ 7 nm. Therefore, the fact that BTMSE can induce the formation of tubular nanostructures but TEOS induces the formation of 2D hexagonal mesostructure suggests the dominant role of the silane precursor on the morphology of the nanohybrids, which is because of the slower hydrolysis/condensation rate and stronger hydrophobicity and rigidity of BTMSE with respect to TEOS.^[31]

Low- and wide-angle XRD patterns of $7.2\text{ArSO}_3\text{H-Si(Et)Si-Ph-NTs}$, $7.3\text{ArSO}_3\text{H-Si(Et)Si-NTs}$, and $6.7\text{PrSO}_3\text{H-SBA-15}$ were measured to characterize their crystal phases (Figure S1). The pattern of $6.7\text{PrSO}_3\text{H-SBA-15}$ displays an intense diffraction peak at $2\theta = 0.98^\circ$ and two weak peaks at $2\theta = 1.64$ and 1.89° , which are indexed as the (100), (110), and (200) Bragg reflections of a 2D hexagonal $p6mm$ structure. In the patterns of $7.2\text{ArSO}_3\text{H-Si(Et)Si-Ph-NTs}$ and $7.3\text{ArSO}_3\text{H-Si(Et)Si-NTs}$, the (100) peak is less intense and the (110) and (200) diffraction peaks are no longer present (Figure S1a). This indicates that $6.7\text{PrSO}_3\text{H-SBA-15}$ possesses a long-range structural ordering, but the pore channels of $7.2\text{ArSO}_3\text{H-Si(Et)Si-Ph-NTs}$ and $7.3\text{ArSO}_3\text{H-Si(Et)Si-NTs}$ are arranged randomly. The results are

Table 1. Textural parameters, acid site density, inner and outer diameter, and wall thickness of the organosulfonic acid functionalized silica materials.

Catalyst	$S_{\text{BET}}^{\text{[a]}}$ [m^2g^{-1}]	$D_p^{\text{[a]}}$ [nm]	$V_p^{\text{[a]}}$ [cm^3g^{-1}]	$A_{\text{titration}}^{\text{[b]}}$ [$\mu\text{eq}(\text{H}^+)\text{g}^{-1}$]	Inner diameter ^[c] [nm]	Outer diameter ^[c] [nm]	Wall thickness ^[c] [nm]
$4.8\text{ArSO}_3\text{H-Si(Et)Si-Ph-NTs}$	731	5.5/44.7	1.28	792	5	11	3
$7.2\text{ArSO}_3\text{H-Si(Et)Si-Ph-NTs}$	694	5.0/30.5	1.19	1140	5	11	3
$8.2\text{ArSO}_3\text{H-Si(Et)Si-Ph-NTs}$	584	5.0/46.0	1.14	1368	5	11	3
$7.3\text{ArSO}_3\text{H-Si(Et)Si-NTs}$	761	5.6/45.3	1.35	1164	5	11	3
$6.8\text{PrSO}_3\text{H-Si(Et)Si-NTs}$	726	5.4/28.9	1.38	1067	5	11	3
$6.7\text{PrSO}_3\text{H-SBA-15}$	770	7.6	1.01	1056	–	–	–
$\text{Si(Et)Si NT}^{\text{[d]}}$	838	5.1/31.7	1.73	–	–	–	–
Amberlyst-15 ^[e]	50	–	–	4800	–	–	–

[a] Surface area (S_{BET}) was calculated using the BET equation; Pore diameter (D_p) was calculated using BJH desorption branch of the isotherms; Pore volume (V_p) was accumulated up to $P/P_0 = 0.99$. [b] From titration with NaOH solution (0.0046 mol L^{-1}). [c] The data were estimated by the TEM images. [d] Data from Ref. [25]. [e] Data from Ref. [34].

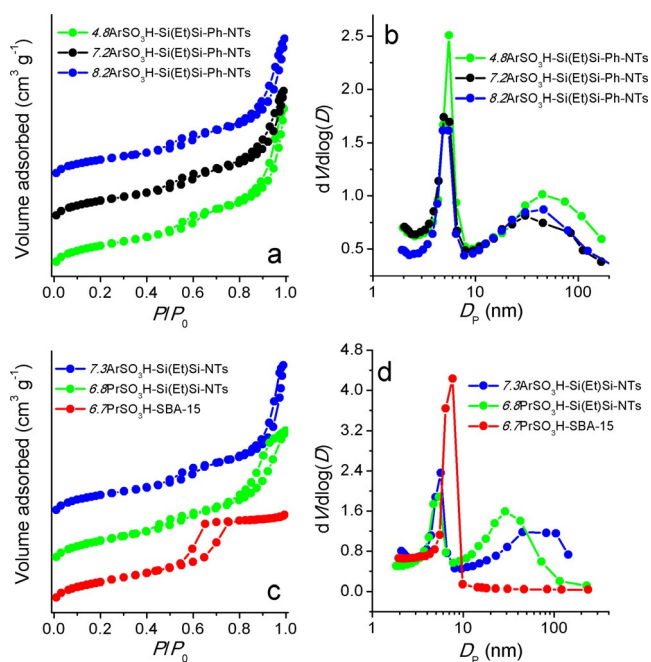


Figure 2. a, c) N_2 gas adsorption–desorption isotherms and b, d) BJH pore size distribution profiles of various SO_3H -based hybrid catalysts.

consistent with the TEM observations. From the wide-angle XRD patterns of $7.2ArSO_3H-Si(Et)Si-Ph-NTs$, $7.3ArSO_3H-Si(Et)Si-NTs$, and $6.7PrSO_3H-SBA-15$ (Figure S1b) it is found that the tested samples exhibit an amorphous crystal phase regardless of the morphology.

The textural properties of all the tested materials, which were characterized by using N_2 physisorption measurements, support the above TEM and XRD measurements. The N_2 sorption isotherms and Barrett–Joyner–Halenda (BJH) pore size distribution curves of the $ArSO_3H-Si(Et)Si-Ph-NTs$ materials with various SO_3H loadings are shown in Figure 2a and b, respectively. The three tested $ArSO_3H-Si(Et)Si-Ph-NTs$ (regardless of SO_3H loadings) show similar N_2 sorption isotherms that feature two capillary condensation steps at $P/P_0=0.45–0.75$ and $0.80–0.99$. Therefore, $ArSO_3H-Si(Et)Si-Ph-NTs$ possesses a bimodal pore structure. From the combination of this result with the pore size distribution curves (Figure 2b) and the calculated textural parameters (Table 1), it is inferred that the primary pores of $ArSO_3H-Si(Et)Si-Ph-NTs$ (5.5–5.0 nm, depending on SO_3H loadings) are well distributed and feature narrow curves, which correspond to the uniform hollow interior of the nanohybrids. The secondary pores (30.5–46.0 nm) are distributed unevenly and feature broader curves, which correspond to the void space between the loosely packed tubular nanoparticles.^[25,31,32] The three $ArSO_3H-Si(Et)Si-Ph-NTs$ materials possess large BET surface areas and high pore volumes, and the BET surface area (731, 694, and $584\text{ m}^2\text{ g}^{-1}$) and pore volume (1.28 , 1.19 , and $1.14\text{ cm}^3\text{ g}^{-1}$) of $ArSO_3H-Si(Et)Si-Ph-NTs$ decrease gradually with an increase of the SO_3H loading from 4.8 to 7.2 and 8.2 wt%. However, the introduction of a suitable amount of arenesulfonic acid groups (e.g., lower than 10 wt%) does not influence the porosity of $ArSO_3H-Si(Et)Si-Ph-NTs$ significantly,

and they still exhibit excellent textural properties that are favorable for the catalytic reactions. Additionally, the $ArSO_3H$ -site-confined 1D hollow interior of the tubular nanohybrids can act as a nanoreactor for the esterification or ethanolysis reactions, which ensures efficient reactant diffusion and acid site accessibility during the reaction.

$7.3ArSO_3H-Si(Et)Si-NTs$ and $6.8PrSO_3H-Si(Et)Si-NTs$ without phenyl groups exhibit the same type of N_2 sorption isotherms and BJH pore size distribution curves to the $ArSO_3H-Si(Et)Si-Ph-NTs$ nanohybrids (Figure 2c and d), which further indicates that 1D hollow tubular nanohybrids have a bimodal pore structure that is contributed to by both the hollow interior and void space of the nanohybrids. As expected, both the nanohybrids exhibit a larger BET surface area (761 and $726\text{ m}^2\text{ g}^{-1}$) and higher pore volume (1.35 and $1.38\text{ cm}^3\text{ g}^{-1}$) than $ArSO_3H-Si(Et)Si-Ph-NTs$ (Table 1).

Compared with ethane-bridged organosilica nanotubes ($Si(Et)Si$ NTs; BET surface area of $838\text{ m}^2\text{ g}^{-1}$ and pore volume of $1.73\text{ cm}^3\text{ g}^{-1}$; Table 1), various organosulfonic acid functionalized silica materials exhibited a smaller BET surface area and lower pore volume. Moreover, for the three $ArSO_3H-Si(Et)Si-Ph-NTs$, their BET surface area and pore volume decrease gradually as the $ArSO_3H$ loading increases. Additionally, at similar $ArSO_3H$ loadings, the BET surface area and pore volume of the bifunctional $7.2ArSO_3H-Si(Et)Si-Ph-NTs$ is lower than that of monofunctionalized $7.3ArSO_3H-Si(Et)Si-NTs$. Therefore, it is inferred that most of the $ArSO_3H$ and terminal phenyl groups of the $ArSO_3H-Si(Et)Si-Ph-NTs$ were confined inside the nanotubes as 1D tubular $ArSO_3H-Si(Et)Si-Ph-NTs$ possess a large fraction of voids in the interior, which resulted in the partial blocking of the tubular channel of the nanohybrids. Consequently, the BET surface area and pore volume of the $ArSO_3H-Si(Et)Si-NTs$ and $ArSO_3H-Si(Et)Si-Ph-NTs$ decrease in comparison to that of pure $Si(Et)Si$ NTs.

$6.7PrSO_3H-SBA-15$ exhibits a type IV isotherm with a H1 hysteresis loop, which signifies that the material possesses a 2D hexagonal ordered mesostructure (Figure 2c and d), and the highly ordered mesostructure leads to the extremely large BET surface area ($770\text{ m}^2\text{ g}^{-1}$) and large pore diameter (7.6 nm) of $6.7PrSO_3H-SBA-15$. However, its pore volume ($1.01\text{ cm}^3\text{ g}^{-1}$) is somewhat lower than that of its tubular counterparts, such as $7.2ArSO_3H-Si(Et)Si-Ph-NTs$ and $6.8PrSO_3H-Si(Et)Si-NTs$.

Surface hydrophobicity

The surface hydrophobicity of the as-prepared organosulfonic acid functionalized silica materials was evaluated by water vapor adsorption measurements, and $7.2ArSO_3H-Si(Et)Si-Ph-NTs$, $7.3ArSO_3H-Si(Et)Si-NTs$, $6.8PrSO_3H-Si(Et)Si-NTs$, and $6.7PrSO_3H-SBA-15$ were selected as representative samples (Figure 3). Based on previous work,^[27] the determined water vapor adsorption isotherms, and the N_2 gas adsorption isotherms, the degree of the surface hydrophobicity of the tested nanohybrids is estimated by the ratio of the water vapor uptake volume (V_{H_2O}) to the N_2 uptake volume (V_{N_2}) measured at $P/P_0=0.15$. This value, which is denoted as $X_{0.15}$, is a good standard to evaluate the surface hydrophobicity of the tested

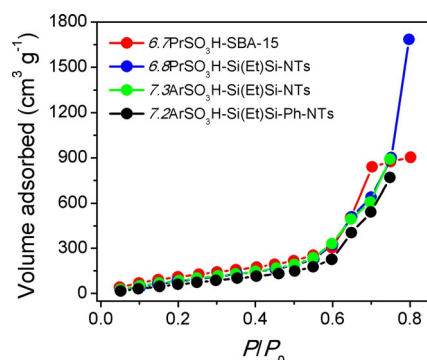


Figure 3. Water vapor adsorption isotherms of various SO_3H -based hybrid catalysts.

nanohybrids if we consider factors that include the adsorption ability for water molecules and the porosity properties of the nanohybrids simultaneously. A lower $x_{0.15}$ value indicates that the surface of the nanohybrids is more hydrophobic. Herein, the calculated $x_{0.15}$ value of 7.2ArSO₃H-Si(Et)Si-Ph-NTs, 7.3ArSO₃H-Si(Et)Si-NTs, 6.8PrSO₃H-Si(Et)Si-NTs, and 6.7PrSO₃H-SBA-15 is 0.26, 0.36, 0.37, and 0.48, respectively. Therefore, multifunctional 7.2ArSO₃H-Si(Et)Si-Ph-NTs exhibits a higher surface hydrophobicity than the other tested SO_3H -based hybrid catalysts. This suggests that the incorporation of the right amount of terminal phenyl groups into the framework of the multifunctional hybrid catalysts can indeed improve the surface hydrophobicity. 6.7PrSO₃H-SBA-15 possesses the lowest surface hydrophobicity because of the lack of hydrophobic organic groups in the framework.

Composition and structural information

The structural integrity of the silica/carbon framework and the incorporated organosulfonic acid and phenyl groups in the as-prepared organic-inorganic hybrid nanotubes were studied by using IR spectroscopy (Figure S2), ²⁹Si magic-angle spinning (MAS) NMR spectroscopy (Figure 4a), and ¹³C cross-polarization (CP) MAS (Figure 4b) NMR spectroscopy.

IR spectra of Si(Et)Si NTs, 7.3ArSO₃H-Si(Et)Si-NTs, and 7.2ArSO₃H-Si(Et)Si-Ph-NTs are presented in Figure S2. For Si(Et)Si NTs, the following characteristic vibrational peaks are detected. The peaks positioned at $\tilde{\nu}=2979$, 2894, and 1273 cm^{-1} are ascribed to vibrations of the C–H bond within the ethane-bridged organosilica framework, whereas the peaks positioned at $\tilde{\nu}=1416$ and 1100 cm^{-1} originate from Si–C vibrations of the silica/carbon framework. The peak situated at $\tilde{\nu}=1030$ cm^{-1} comes from Si–O vibrations of the silica/carbon framework. After the functionalization of the organosilica nanotubes with ArSO₃H groups, 7.3ArSO₃H-Si(Et)Si-NTs was obtained. In addition to the aforementioned six vibrational peaks related to Si(Et)Si NTs, some new absorption peaks were found in the spectrum of 7.3ArSO₃H-Si(Et)Si-NTs. A group of weak peaks appeared in the range of $\tilde{\nu}=1700$ –1600 cm^{-1} that originate from the stretching vibrations of the ring framework or the deformation vibrations of C–H bonds of benzene.^[33] The

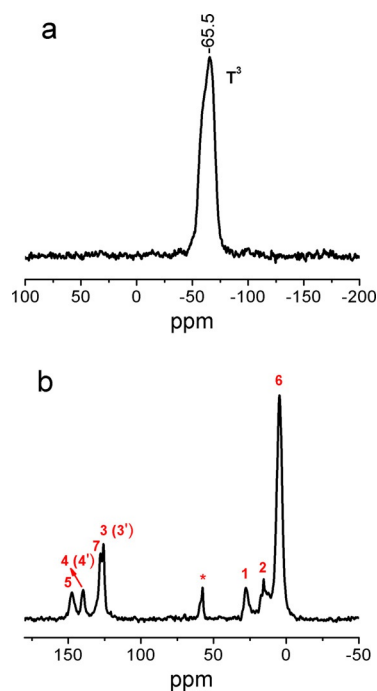


Figure 4. a) ²⁹Si MAS and b) ¹³C CP-MAS NMR spectra of 7.2ArSO₃H-Si(Et)Si-Ph-NTs.

peak at $\tilde{\nu}=590$ cm^{-1} is ascribed to SO_3H vibrations.^[34] The IR spectrum of 7.2ArSO₃H-Si(Et)Si-Ph-NTs is similar to that of 7.3ArSO₃H-Si(Et)Si-NTs, but the vibrational absorption in the range of $\tilde{\nu}=1700$ –1600 cm^{-1} is stronger, which implies the successful introduction of phenyl groups into the silica/carbon framework of the nanohybrids. However, because of the interference of the strong IR absorption of the Si–C and Si–O bonds, the characteristic IR absorptions that originate from the O=S=O and S=O stretching vibrations ($\tilde{\nu}=1034$ and 1005 cm^{-1})^[35] as well as ring framework or C–H bonds of benzene are hardly observed. Therefore, it is difficult to confirm the introduction of ArSO₃H and phenyl groups into the silica/carbon framework.

To further confirm the structural integrity of the silica/carbon framework and the incorporated organosulfonic acid or phenyl groups and to study the interaction between the functionalities and silica/carbon framework in as-prepared hybrid nanotubes, ²⁹Si MAS NMR and ¹³C CP-MAS NMR spectra were measured for 7.2ArSO₃H-Si(Et)Si-Ph-NTs as a representative sample. In the ²⁹Si MAS NMR spectrum, the characteristic resonance at $\delta=-65.5$ ppm is assigned to T³ organosiloxane species [–CH₂CH₂–Si(OSi)₃] within the ethane-bridged organosilica framework, which indicates that the ethane-bridged organosilica framework (–Si–O_{1.5}–Si–CH₂–CH₂–Si–O_{1.5}–) has been fabricated successfully. Additionally, the incorporation of terminal phenyl groups can greatly reduce the amount of T² [–CH₂CH₂–Si(OSi)₂(OH)] and T¹ [–CH₂CH₂–Si(OSi)(OH)₂] organosiloxane species within the ethane-bridged organosilica framework to lead to the enhancement of the surface hydrophobicity of the nanohybrids. Additionally, the resonance signals that correspond to inorganic SiO₄ species such as Q³ [Si(OSi)₃(OH)]; $\delta=$

–90 ppm] and Q^4 [$Si(OSi)_4$; $\delta = -120$ ppm] were not found, which implies that the cleavage of the Si–C bond in the silica/carbon framework has been avoided.

In the ^{13}C CP-MAS NMR spectrum of $7.2ArSO_3H-Si(Et)Si-Ph-NTs$, five signals at $\delta = 15.6, 27.7, 125.7, 139.8,$ and 147.3 ppm belong to the five types of carbon species of the arenesulfonic acid groups (C^1-C^5 in Figure 4b), in which the first two signals originate from the methylene carbon atoms (C^1 and C^2 in Figure 4b) of the $ArSO_3H$ groups, and the last three signals correspond to the aromatic carbon atoms ($C^3, C^4,$ and C^5 in Figure 4b) of the $ArSO_3H$ groups.^[36] The most intense signal at $\delta = 4.7$ ppm is assigned to the carbon species of the bridging ethyl groups of the silica/carbon framework (C^6 in Figure 4b).^[37] Additionally, three signals at $\delta = 125.7, 127.8,$ and 139.8 ppm belong to aromatic carbon species of the terminal phenyl groups ($C^{3'}, C^{7'},$ and $C^{4'}$ in Figure 4b), in which two signals ($C^{3'}$ and $C^{4'}$) are covered by the two signals that correspond to aromatic carbon atoms (C^3 and C^4) of the $ArSO_3H$ groups. These results confirm that both $ArSO_3H$ and phenyl groups were successfully introduced into the silica/carbon framework.

Based on the above discussion, the walls of the ethane-bridged organosilica nanotubes modified by arenesulfonic acid and terminal phenyl groups are composed of a covalently bonded organic–inorganic framework of $C_6H_5-Si-O-Si-CH_2-CH_2-Si-O-Si-CH_2-CH_2-C_6H_4-SO_3H$, in which the $-Si-CH_2-CH_2-Si-$ moieties originate from BTMSE, the $-Si-CH_2-CH_2-C_6H_4-SO_3H$ fragments come from CSPTMS, and the C_6H_5-Si- units arise from PhTMS.

Brønsted acid site density

The Brønsted acid site density of the as-prepared organosulfonic acid functionalized silica materials was determined by titration with dilute NaOH solution ($0.0046 \text{ mol L}^{-1}$; Table 1). For the three $ArSO_3H-Si(Et)Si-Ph-NTs$ materials, their Brønsted acid site density [$792, 1140,$ and $1368 \mu\text{eq}(\text{H}^+) \text{g}^{-1}$] increases gradually with the increasing SO_3H loading (4.8, 7.2, and 8.2 wt%). Additionally, at a similar SO_3H loading (6.7 to 7.3 wt%), $7.2ArSO_3H-Si(Et)Si-Ph-NTs$ [$1140 \mu\text{eq}(\text{H}^+) \text{g}^{-1}$], $7.3ArSO_3H-Si(Et)Si-NTs$ [$1164 \mu\text{eq}(\text{H}^+) \text{g}^{-1}$], $6.8PrSO_3H-Si(Et)Si-NTs$ [$1067 \mu\text{eq}(\text{H}^+) \text{g}^{-1}$], and $6.7PrSO_3H-SBA-15$ [$1056 \mu\text{eq}(\text{H}^+) \text{g}^{-1}$] possess similar Brønsted acid site densities, regardless of the differences in morphology and surface hydrophobicity. This suggests that the Brønsted acid site density of the as-prepared organosulfonic acid functionalized silica materials is dominated by their SO_3H loading.

Catalytic performance

Esterification of levulinic acid

The heterogeneous acid catalytic activity of the as-prepared $ArSO_3H-Si(Et)Si-Ph-NTs$ nanohybrids was firstly evaluated for the esterification of levulinic acid with ethanol to yield ethyl levulinate at a levulinic acid-to-ethanol molar ratio of 1:7, 2 wt% catalyst, 78°C , and atmospheric pressure.

Firstly, the influence of SO_3H loading on the esterification activity was studied. The three tested $ArSO_3H-Si(Et)Si-Ph-NTs$ nanohybrids follow the activity order $7.2ArSO_3H-Si(Et)Si-Ph-NTs > 8.2ArSO_3H-Si(Et)Si-Ph-NTs > 4.8ArSO_3H-Si(Et)Si-Ph-NTs$ (Figure 5). For example, after the reaction was performed for 3 h, the yield of ethyl levulinate reached 94.4% ($7.2ArSO_3H-Si(Et)Si-Ph-NTs$), 84.5% ($8.2ArSO_3H-Si(Et)Si-Ph-NTs$), and 82.5% ($4.8ArSO_3H-Si(Et)Si-Ph-NTs$).

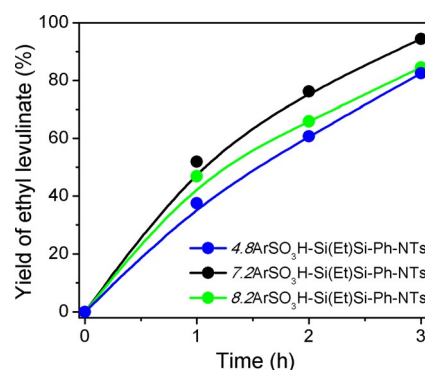


Figure 5. Catalytic activity of $ArSO_3H-Si(Et)Si-Ph-NTs$ hybrid catalysts with various SO_3H group loadings in the esterification of levulinic acid with ethanol. Levulinic acid 9.85 mmol; ethanol 68.95 mmol; 2 wt% catalyst; 78°C ; atmospheric pressure.

Subsequently, the esterification activity of the most active catalyst, $7.2ArSO_3H-Si(Et)Si-Ph-NTs$, was compared with that of $7.3ArSO_3H-Si(Et)Si-NTs$, $6.8PrSO_3H-Si(Et)Si-NTs$, and $6.7PrSO_3H-SBA-15$. Homogeneous H_2SO_4 and macroreticular Amberlyst-15 were also tested for comparison. The yields of ethyl levulinate in the Brønsted acid catalyzed esterification reaction are shown in Figure 6a. $7.2ArSO_3H-Si(Et)Si-Ph-NTs$ is much more catalytically active than $7.3ArSO_3H-Si(Et)Si-NTs$ at a similar SO_3H loading level, and $7.3ArSO_3H-Si(Et)Si-NTs$ is more active than $6.8PrSO_3H-Si(Et)Si-NTs$. As for 2D ordered mesoporous $6.7PrSO_3H-SBA-15$, its esterification activity is lower than that of the hollow tubular $6.8PrSO_3H-Si(Et)Si-NTs$. For the $7.2ArSO_3H-Si(Et)Si-Ph-NTs$ -, $7.3ArSO_3H-Si(Et)Si-NTs$ -, $6.8PrSO_3H-Si(Et)Si-NTs$ -, and $6.7PrSO_3H-SBA-15$ -catalyzed esterification reaction, the yield of ethyl levulinate reached 94.4, 81.5, 72.6, and 64.7%, respectively, after the reaction proceeded for 3 h. In the H_2SO_4 -catalyzed esterification reaction, the yield of ethyl levulinate reached almost 100% after 1 h. However, H_2SO_4 suffers from disadvantages such as corrosion, difficulty in separation, and acid-waste generation, which lead to its uncompetitiveness with respect to solid acids. Amberlyst-15 exhibited a lower esterification activity than $7.2ArSO_3H-Si(Et)Si-Ph-NTs$, and the yield of ethyl levulinate reached 75.1% after 3 h.

As the tested acid catalysts possess different acid site densities, their esterification activities were further compared in terms of the yield of ethyl levulinate per acid site of each catalyst (turnover frequency; TOF [h^{-1}]) after 1 h. From the results shown in Figure 6b, it is found that the tested catalysts follow the TOF order $7.2ArSO_3H-Si(Et)Si-Ph-NTs$ (51.0 h^{-1}) $>$ $7.3ArSO_3H-Si(Et)Si-NTs$ (38.8 h^{-1}) $>$ $6.8PrSO_3H-Si(Et)Si-NTs$ (35.0 h^{-1}) $>$

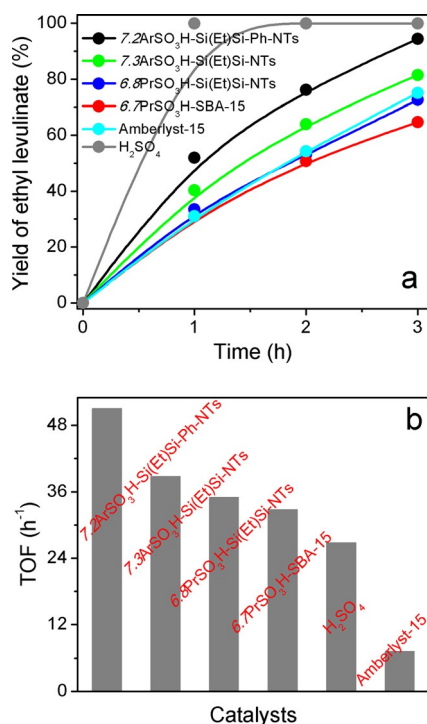


Figure 6. Catalytic activity of various Brønsted acid catalysts for the esterification of levulinic acid with ethanol to yield ethyl levulinate. a) Yield of ethyl levulinate and b) TOF after 1 h. Levulinic acid 9.85 mmol; ethanol 68.95 mmol; 2 wt% catalyst; 78 °C; atmospheric pressure.

6.7PrSO₃H-SBA-15 (32.8 h⁻¹) > H₂SO₄ (26.8 h⁻¹) > Amberlyst-15 (7.2 h⁻¹). The lower TOF value but higher yield of H₂SO₄ is because of its high Brønsted acid site density.^[38] Therefore, as-prepared ArSO₃H-Si(Et)Si-Ph-NTs showed excellent heterogeneous acid catalytic activity in the esterification reaction.

Ethanolysis of furfuryl alcohol

The synthesis of ethyl levulinate by the direct esterification of levulinic acid with ethanol suffers from some drawbacks such as the high cost of the raw material and the production of water as a byproduct. The ethanolysis of furfuryl alcohol is an economical method to synthesize ethyl levulinate.

Firstly, the ethanolysis activity of various ArSO₃H-Si(Et)Si-Ph-NTs nano-hybrids with SO₃H loadings of 4.8, 7.2, and 8.2 wt% was tested at a furfuryl alcohol-to-ethanol molar ratio of 1:60, 1.5 wt% catalyst, and 120 °C. The three ArSO₃H-Si(Et)Si-Ph-NTs nano-hybrids showed remarkably high ethanolysis activities, and the activity was in proportion to the SO₃H loading (Figure 7). For example, after 120 min, the yield of ethyl levulinate reached 73.0% (4.8ArSO₃H-Si(Et)Si-Ph-NTs), 85.0% (7.2ArSO₃H-Si(Et)Si-Ph-NTs), and 84.5% (8.2ArSO₃H-Si(Et)Si-Ph-NTs).

Subsequently, the ethanolysis activity of the most active catalyst, 7.2ArSO₃H-Si(Et)Si-Ph-NTs, was compared with that of 7.3ArSO₃H-Si(Et)Si-NTs, 6.8PrSO₃H-Si(Et)Si-NTs, and 6.7PrSO₃H-SBA-15. H₂SO₄ and macroreticular Amberlyst-15 were also evaluated under the same conditions. The four as-prepared organosulfonic acid functionalized silica materials followed the

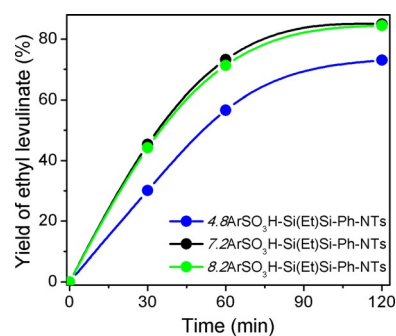


Figure 7. Catalytic activity of ArSO₃H-Si(Et)Si-Ph-NTs hybrid catalysts with various SO₃H group loadings for the ethanolysis of furfuryl alcohol to ethyl levulinate. Furfuryl alcohol 1.15 mmol; ethanol 69.00 mmol; 1.5 wt% catalyst, 120 °C.

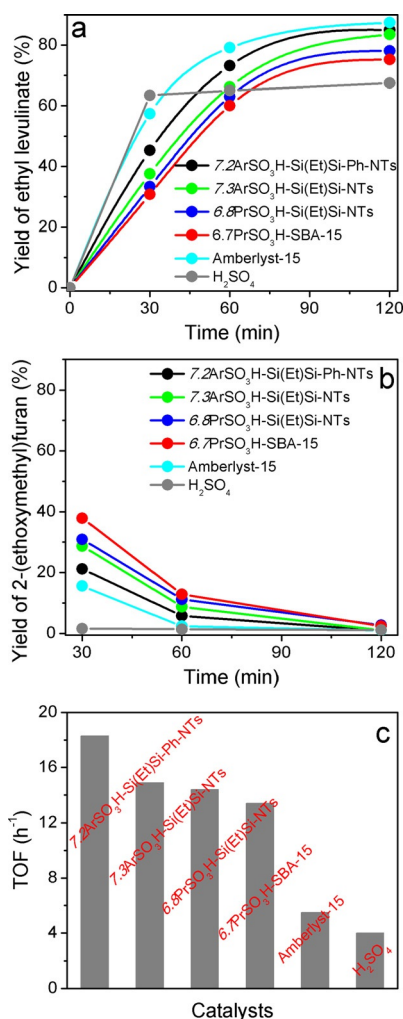


Figure 8. Catalytic activity of various Brønsted acid catalysts for the ethanolysis of furfuryl alcohol to ethyl levulinate. a) Yield of ethyl levulinate, b) yield of 2-(ethoxymethyl)furan, and c) yield of ethyl levulinate per acid site (TOF [h⁻¹]) after 30 min. Furfuryl alcohol 1.15 mmol; ethanol 69.00 mmol; 1.5 wt% catalyst, 120 °C.

ethanolysis activity (evaluated by the yield of ethyl levulinate) order of 7.2ArSO₃H-Si(Et)Si-Ph-NTs > 7.3ArSO₃H-Si(Et)Si-NTs > 6.8PrSO₃H-Si(Et)Si-NTs > 6.7PrSO₃H-SBA-15 (Figure 8a), which is similar to the order of their esterification activity. Additionally,

Amberlyst-15 is the most active among all of the tested acid catalysts. For the Amberlyst-15-, $7.2\text{ArSO}_3\text{H-Si(Et)Si-Ph-NTs}$ -, $7.3\text{ArSO}_3\text{H-Si(Et)Si-NTs}$ -, $6.8\text{PrSO}_3\text{H-Si(Et)Si-NTs}$ -, and $6.7\text{PrSO}_3\text{H-SBA-15}$ -catalyzed ethanolysis reactions, the yield of ethyl levulinate was 87.4, 85.0, 83.5, 78.1, and 75.2%, respectively, after 120 min. During the initial stage of the ethanolysis reaction, the yield of ethyl levulinate increased rapidly in the homogeneous H_2SO_4 -catalyzed reaction system. For example, the yield of ethyl levulinate reached 63.5% after 30 min. However, with a further increase of the reaction time to 120 min, the ethanolysis activity remained unchanged. This may be because many oligomeric condensation products of furfuryl alcohol can be formed in the H_2SO_4 -catalyzed ethanolysis reaction because of the extremely high Brønsted acid strength and strong surface hydrophilicity of H_2SO_4 .^[6] The highest yield of ethyl levulinate obtained for the Amberlyst-15-catalyzed ethanolysis reaction is because of its much higher Brønsted acid site density [$4800 \mu\text{eq}(\text{H}^+)\text{g}^{-1}$] and low surface hydrophilicity, which can provide many more acid sites for the target reaction and decrease the absorption of oligomeric condensation byproducts as well.

GC-MS analysis confirms that the intermediate 2-(ethoxymethyl)furan was formed during the conversion of furfuryl alcohol to ethyl levulinate. The yield of 2-(ethoxymethyl)furan decreased gradually with the increase of the reaction time from 30 to 120 min (Figure 8b), which implies that 2-(ethoxymethyl)furan continued to be converted into ethyl levulinate. The formation rate for 2-(ethoxymethyl)furan over various SO_3H -based catalysts is Amberlyst-15 > $7.2\text{ArSO}_3\text{H-Si(Et)Si-Ph-NTs}$ > $7.3\text{ArSO}_3\text{H-Si(Et)Si-NTs}$ > $6.8\text{PrSO}_3\text{H-Si(Et)Si-NTs}$ > $6.7\text{PrSO}_3\text{H-SBA-15}$. However, for the homogeneous H_2SO_4 -catalyzed ethanolysis reaction, 2-(ethoxymethyl)furan was hardly formed, which suggests that ethyl levulinate and the oligomeric condensation byproducts were formed rapidly in the H_2SO_4 -catalyzed ethanolysis process.

If we consider the different acid site densities of the various acid catalysts tested, the ethanolysis activity was compared in terms of the yield of ethyl levulinate per acid site of each catalyst (TOF) after 30 min. The tested catalysts follow the TOF order $7.2\text{ArSO}_3\text{H-Si(Et)Si-Ph-NTs}$ (18.3 h^{-1}) > $7.3\text{ArSO}_3\text{H-Si(Et)Si-NTs}$ (14.9 h^{-1}) > $6.8\text{PrSO}_3\text{H-Si(Et)Si-NTs}$ (14.4 h^{-1}) > $6.7\text{PrSO}_3\text{H-SBA-15}$ (13.4 h^{-1}) > Amberlyst-15 (5.5 h^{-1}) > H_2SO_4 (4.0 h^{-1}) (Figure 8c). The lower TOF value and higher yield of ethyl levulinate for the H_2SO_4 - and Amberlyst-15-catalyzed ethanolysis reaction is because of the higher Brønsted acid site density. Therefore, $7.2\text{ArSO}_3\text{H-Si(Et)Si-Ph-NTs}$ is still catalytically active in the ethanolysis reaction.

Discussion

The excellent esterification and ethanolysis activity of the $\text{ArSO}_3\text{H-Si(Et)Si-Ph-NTs}$ organic-inorganic hybrid nanocatalysts can be explained by the combination of the strong Brønsted acidity, unique hollow nanotube morphology, excellent porosity properties, and interesting hydrophobic surface.

Firstly, a possible mechanism of the Brønsted acid catalyzed esterification of levulinic acid and the ethanolysis of furfuryl al-

cohol is considered to better understand the excellent acid catalytic activity of the multifunctional $\text{ArSO}_3\text{H-Si(Et)Si-Ph-NTs}$ hybrid nanocatalysts.

In the $\text{ArSO}_3\text{H-Si(Et)Si-Ph-NTs}$ -catalyzed esterification reaction (Scheme S1 a), the strong Brønsted acidity of the catalyst can protonate the carbonyl groups of levulinic acid molecules in the first step to give oxonium ions that are readily attacked by ethanol molecules through an exchange reaction to produce ethyl levulinate molecules after the loss of one hydrogen atom.^[28,39]

The mechanism of the $\text{ArSO}_3\text{H-Si(Et)Si-Ph-NTs}$ -catalyzed ethanolysis reaction is also put forward based on the literature and our previous work^[40,41] as well as the identified intermediates (Scheme S1 b). Similar to the first step in the esterification reaction, the furfuryl alcohol molecules are firstly activated by the Brønsted acid sites, and the activated furfuryl alcohol molecules are attacked by ethanol molecules to form 2-(ethoxymethyl)furan and water. Next, intermediate A is formed by the ring-opening reaction caused by the attack of water molecules on the cyclic oxonium obtained by the protonation of epoxy groups in the presence of Brønsted acid sites. Subsequently, the formation of ethyl levulinate may proceed through the following possible pathways: intermediate A is isomerized with the release of one hydrogen atom to form ethyl levulinate (Path I). Intermediate A is isomerized and the produced compound is activated by the Brønsted acid sites. After attack by ethanol molecules, 4,5-diethoxy-5-hydroxypentan-2-one is formed. One ethanol molecule is released from 4,5-diethoxy-5-hydroxypentan-2-one followed by isomerization to form ethyl levulinate; meanwhile, 4,5-diethoxy-5-hydroxypentan-2-one activated by the Brønsted acid sites is further attacked by ethanol molecules, and 4,5,5-triethoxypentan-2-one is formed with the release of water molecules (Path II). Intermediate A is isomerized and the produced compound is activated by the Brønsted acid sites. After attack by ethanol molecules, 4,5,5-triethoxypentan-2-one is formed. After the release of one diethyl ether molecule from 4,5,5-triethoxypentan-2-one followed by isomerization, ethyl levulinate is formed (Path III). In the above reaction processes, the intermediates and byproducts (identified by GC-MS, Table S1 and Figure S3) are produced inevitably. The produced intermediates are 2-(ethoxymethyl)furan (main), 4,5-diethoxy-5-hydroxypentan-2-one (minor), and 4,5,5-triethoxypentan-2-one (minor), whereas the byproducts found are diethyl ether (nonproductive consumption of ethanol) and some oligomeric products of furfuryl alcohol such as difuran-2-ylmethane, 2-[(furan-2-ylmethoxy)methyl]furan, and 2,5-bis(furan-2-ylmethyl)furan.

The strong Brønsted acidity of the SO_3H -based silica nanohybrids, which includes the Brønsted acid site density and acid strength, plays a key role to ensure that both of the target reactions proceed at a considerably fast rate. For the $4.8\text{ArSO}_3\text{H-Si(Et)Si-Ph-NTs}$ - and $7.2\text{ArSO}_3\text{H-Si(Et)Si-Ph-NTs}$ -catalyzed esterification and ethanolysis reactions, the lower catalytic activity of $4.8\text{ArSO}_3\text{H-Si(Et)Si-Ph-NTs}$ than $7.2\text{ArSO}_3\text{H-Si(Et)Si-Ph-NTs}$ is mainly because of the lower Brønsted acid site density of the former. Phenyl-free $7.3\text{ArSO}_3\text{H-Si(Et)Si-NTs}$ and $6.8\text{PrSO}_3\text{H-Si(Et)Si-NTs}$ both possess a 1D hollow tubular nanostructure

and have similar Brønsted acid site densities and textural properties, but the slightly higher catalytic activity of 7.3ArSO₃H-Si(Et)Si-NTs than 6.8PrSO₃H-Si(Et)Si-NTs is because of their different acid strength, which is mainly determined by the micro-environment of the SO₃H sites in both catalysts.^[42,43] For 7.3ArSO₃H-Si(Et)Si-NTs, phenyl groups in the arenesulfonic acid groups can provide a stronger electron-withdrawing environment than the propyl groups in the propylsulfonic acid group of 6.8PrSO₃H-Si(Et)Si-NTs, which leads to the higher Brønsted acid strength and, thereby, higher catalytic activity of 7.3ArSO₃H-Si(Et)Si-NTs.

Additionally, the heterogeneous acid catalytic activity of organosulfonic acid functionalized silica materials is also dominated to some extent by their morphological characteristics and porosity properties. The materials with a 1D hollow tubular nanostructure can serve as nanoreactors to permit esterification or ethanolysis reaction to take place inside. Accordingly, the diffusion path of the reactants and products was decreased to lead to the increased accessibility of SO₃H sites to levulinic acid or furfuryl alcohol molecules in comparison to that of their 2D hexagonal mesostructured counterpart 6.7PrSO₃H-SBA-15. Moreover, the mass transfer of the reactants and products can be speeded up because they were confined in the interior of nanotubes. Additionally, unique morphological characteristics lead to the excellent porosity properties of the tubular nanohybrids that include the large BET surface area and high pore volume, which can provide a high population of SO₃H sites for the reactions. These three factors ensure that ArSO₃H-Si(Et)Si-Ph-NTs show a higher esterification or ethanolysis activity than 6.7PrSO₃H-SBA-15 at a similar SO₃H loading.

The slightly lower esterification and ethanolysis activity of 8.2ArSO₃H-Si(Et)Si-Ph-NTs than 7.2ArSO₃H-Si(Et)Si-Ph-NTs is because of the decreased BET surface area and pore volume of 8.2ArSO₃H-Si(Et)Si-Ph-NTs although it has a higher Brønsted acid site density.

Finally, the enhanced surface hydrophobicity of the ArSO₃H-Si(Et)Si-Ph-NTs with respect to ArSO₃H-Si(Et)Si-NT is critical to improve the esterification and ethanolysis activity. In the esterification reaction, water was produced as a byproduct and adsorb favorably on the surface of the hydrophilic SO₃H-based silica catalysts, which can inhibit the esterification reaction to some extent.^[44] Moreover, some of the yielded ethyl levulinate can be hydrolyzed by water. These problems can be alleviated by the functionalization of sulfonic acid based silica materials with hydrophobic bridging ethyl and terminal phenyl groups, which can selectively create an unsuitable environment for water molecules and lead them to escape easily from the catalyst surface. Additionally, the incorporation of terminal phenyl groups also inhibits the deactivation of the adjacent sulfonic acid sites because of the strong adsorption of water molecules on the catalyst surface; furthermore, the terminal phenyl groups can effectively reduce the number of silanol groups on the surface of the organic-inorganic hybrid nanotubes to lead to the enhancement of the acid strength of the sulfonic acid groups by inhibiting their interaction with the surface.^[45] Notably, the acid catalytic activity of 7.2ArSO₃H-Si(Et)Si-Ph-NTs is higher than that of 7.3ArSO₃H-Si(Et)Si-NTs, although the latter

possesses a larger BET surface area. This demonstrates that the terminal phenyl groups appear to influence the esterification activity of SO₃H-based organic-inorganic hybrid catalysts.

The ethanolysis reaction occurred under solvothermal conditions so it is inevitable that oligomeric byproducts such as furan-2-ylmethane, 2-[(furan-2-ylmethoxy)methyl]furan, and 2,5-bis(furan-2-ylmethyl)furan (identified by GC-MS; Table S1 and Figure S3) were produced by the self-polymerization of furfuryl alcohol. These oligomeric byproducts were adsorbed onto the surface of SO₃H-based silica catalysts because of the interaction with the silanol groups. Accordingly, the ethanolysis reaction was inhibited to some degree, and the regeneration of the catalysts became more difficult. After the incorporation of both bridging ethyl groups and terminal phenyl groups into the framework of the catalysts, the adsorption of oligomeric products on the adjacent sulfonic acid sites can be avoided effectively because of the enhanced surface hydrophobicity, which leads to the higher ethanolysis activity of 7.2ArSO₃H-Si(Et)Si-Ph-NTs than 7.3ArSO₃H-Si(Et)Si-NTs. Additionally, the ethanolysis stability of 7.2ArSO₃H-Si(Et)Si-Ph-NTs was improved (Figure 10).

Regeneration and reusability

The catalytic stability of the anchored acid sites and the reusability of heterogeneous solid acid catalysts in the liquid media have been a major concern from the viewpoint of applications. The reusability of the as-prepared multifunctional ArSO₃H-Si(Et)Si-Ph-NTs hybrid nanocatalysts was, therefore, studied for the esterification of levulinic acid with ethanol, and 7.2ArSO₃H-Si(Et)Si-Ph-NTs was selected as the representative catalyst. The esterification reaction was repeated three times. After each catalytic cycle, the used catalyst was recovered by centrifugation, washed thoroughly with ethanol three times, and dried at 100 °C before the next cycle. 7.2ArSO₃H-Si(Et)Si-Ph-NTs exhibited excellent catalytic stability, and the yield of ethyl levulinate was 94.4 (first run), 93.5 (second run), and 93.9% (third run) after 3 h (Figure 9). This result indicates that as-prepared ArSO₃H-Si(Et)Si-Ph-NTs is catalytically stable and can maintain a similar level of esterification activity at least for three catalytic cycles.

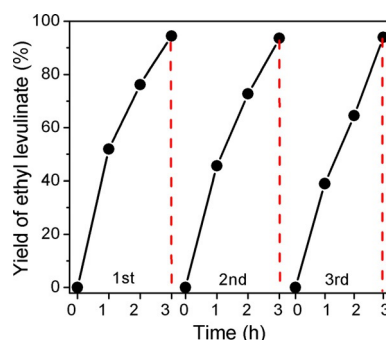


Figure 9. Reusability of the representative 7.2ArSO₃H-Si(Et)Si-Ph-NTs in the esterification of levulinic acid with ethanol. Levulinic acid 9.85 mmol; ethanol 68.95 mmol; 2 wt% catalyst; 3 h; 78 °C; atmospheric pressure.

Subsequently, the reusability of the $\text{ArSO}_3\text{H-Si(Et)Si-Ph-NTs}$ (represented by $7.2\text{ArSO}_3\text{H-Si(Et)Si-Ph-NTs}$) was further evaluated for the ethanolsis of furfuryl alcohol, and the reaction was repeated five times. The nanohybrids maintain a good catalytic stability in the ethanolsis reaction, and the yield of ethyl levulinate was 85.0 (first run), 85.0 (second run), 83.5 (third run), 79.8 (fourth run), and 73.7% (fifth run) after 2 h (Figure 10a).

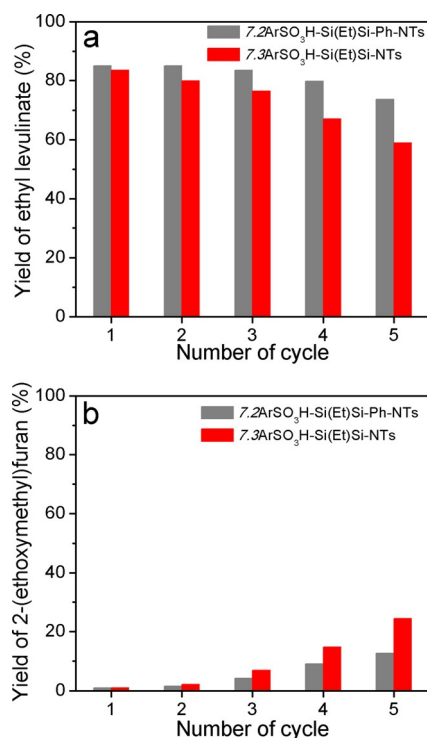


Figure 10. Reusability of $7.2\text{ArSO}_3\text{H-Si(Et)Si-Ph-NTs}$ and $7.3\text{ArSO}_3\text{H-Si(Et)Si-NTs}$ in the ethanolsis of furfuryl alcohol to ethyl levulinate. a) Yield of ethyl levulinate and b) yield of 2-(ethoxymethyl)furan. Furfuryl alcohol 1.15 mmol; ethanol 69.00 mmol; 1.5 wt% catalyst; 120 min; 120°C .

For comparison, the reusability of phenyl-free $7.3\text{ArSO}_3\text{H-Si(Et)Si-NTs}$ was also tested under the same conditions and showed a clear loss of activity (Figure 10a). That is, the yield of ethyl levulinate decreased from 83.5% in the first run to 59.0% in the fifth run in the $7.3\text{ArSO}_3\text{H-Si(Et)Si-NTs}$ -catalyzed ethanolsis reaction. The activity loss observed after the recycling of the SO_3H -based catalysts is caused by the strong adsorption of hydrophilic oligomeric byproducts on the catalyst surface. The problem can be moderated by the incorporation of hydrophobic alkyl groups within the solid acid framework, which can prevent the absorption of the oligomeric byproducts on the catalyst surface effectively. Therefore, $7.2\text{ArSO}_3\text{H-Si(Et)Si-Ph-NTs}$ with two hydrophobic alkyl groups is catalytically more stable than $7.3\text{ArSO}_3\text{H-Si(Et)Si-NTs}$ with one hydrophobic alkyl group.

To further study the influence of the adsorbed oligomeric byproducts on the catalytic activity and stability of $7.2\text{ArSO}_3\text{H-Si(Et)Si-Ph-NTs}$ and $7.3\text{ArSO}_3\text{H-Si(Et)Si-NTs}$, the yield of 2-(ethoxymethyl)furan was determined in the first, second, third, fourth, and fifth catalytic cycles (Figure 10b). The yield of 2-(ethoxymethyl)furan increased as the catalyst was used more

times; moreover, the accumulation of 2-(ethoxymethyl)furan was more serious for phenyl-free $7.3\text{ArSO}_3\text{H-Si(Et)Si-NTs}$ (yield of 1.0, 2.2, 7.0, 14.7, and 24.4%, respectively) with respect to $7.2\text{ArSO}_3\text{H-Si(Et)Si-Ph-NTs}$ (yield of 1.0, 1.6, 4.3, 9.1, and 12.7%, respectively). The ethanolsis of furfuryl alcohol is a multistep reaction, and the formation of 2-(ethoxymethyl)furan is the first step that is a rapid response. The subsequent acidification of 2-(ethoxymethyl)furan to ethyl levulinate is the rate-limiting step. Additionally, the ethanolsis reaction can produce oligomeric byproducts. These hydrophilic oligomeric byproducts were adsorbed on the surface of the monofunctional $\text{ArSO}_3\text{H-Si(Et)Si-NTs}$ and bifunctional $\text{ArSO}_3\text{H-Si(Et)Si-Ph-NTs}$ catalysts, which inhibited the fast conversion of 2-(ethoxymethyl)furan to ethyl levulinate. During the process of catalyst recycling, more and more oligomeric byproducts were adsorbed on the catalyst surface, which in turn led to serious 2-(ethoxymethyl)furan accumulation on the catalyst surface. Consequently, the formation of ethyl levulinate became more difficult as the number of recycling times was increased. The circumstance was more serious for $\text{ArSO}_3\text{H-Si(Et)Si-NTs}$ than for $\text{ArSO}_3\text{H-Si(Et)Si-Ph-NTs}$. Accordingly, more 2-(ethoxymethyl)furan was formed during the $\text{ArSO}_3\text{H-Si(Et)Si-NTs}$ -catalyzed ethanolsis process (Figure 10b), accompanied by a decreased yield of ethyl levulinate (Figure 10a).

Consequently, the formation of more 2-(ethoxymethyl)furan may hinder the further formation of ethyl levulinate. Therefore, it is inferred that the lower yield of ethyl levulinate obtained over $7.3\text{ArSO}_3\text{H-Si(Et)Si-NT}$ than that over $7.2\text{ArSO}_3\text{H-Si(Et)Si-Ph-NTs}$ is because of the decreased catalytic ability for the further formation of the product because of the adsorbance of more oligomeric byproducts; and introduction of the second hydrophobic alkyl group can decrease the adsorption, and thereby, the catalytic activity was restored. In addition, the leaching of the SO_3H groups into the reaction medium was barely detected by inductively coupled plasma optical emission spectroscopy (ICP-OES), which supports the above results.

The excellent reusability of $\text{ArSO}_3\text{H-Si(Et)Si-Ph-NTs}$ is a result of the strong chemical interactions between the arenesulfonic acid groups and the silica/carbon framework; moreover, the surface hydrophobicity of the silica/carbon framework that contains both bridging ethyl and terminal phenyl groups can reduce the acid site deactivation associated with the adsorption of hydrophilic byproducts. Therefore, these SO_3H -based nanohybrids work effectively as recyclable solid acid catalysts in both esterification and ethanolsis reactions.

Conclusions

The design of SO_3H -based organic-inorganic hybrid silica materials with interesting nanostructures and surface hydrophobicity is an effective approach to improve their acid catalytic activity and stability in the synthesis of ethyl levulinate from biomass-derived platform molecules such as levulinic acid and furfuryl alcohol. For this purpose, ethane-bridged organosilica nanotubes functionalized with arenesulfonic acid and phenyl groups ($\text{ArSO}_3\text{H-Si(Et)Si-Ph-NTs}$) were fabricated successfully by a single-step preparation route. The as-prepared $\text{ArSO}_3\text{H-}$

Si(Et)Si-Ph-NTs hybrid nanocatalysts exhibited excellent heterogeneous acid catalytic activity in the synthesis of ethyl levulinate from the esterification of levulinic acid or the ethanolysis of furfuryl alcohol, and the activity outperformed that of their counterparts such as phenyl-free 1D hollow tubular $\text{ArSO}_3\text{H-Si(Et)Si-Ph-NTs}$ without phenyl groups and 2D hexagonal mesoporous $\text{PrSO}_3\text{H-SBA-15}$. This enhanced catalytic activity was because of: i) the 1D hollow tubular morphology of the hybrid nanocatalysts, which can serve as nanoreactors to shorten the diffusion pathway and facilitate mass transfer; and ii) the hydrophobic surface of the hybrid nanocatalysts, which can inhibit the strong adsorption of hydrophilic byproducts on the surface silanol and adjacent organosulfonic acid groups. Both of these factors can improve the accessibility of the acid sites to the substrates and, thereby, the catalytic activity. Importantly, the enhanced surface hydrophobicity led to the better catalytic stability of $\text{ArSO}_3\text{H-Si(Et)Si-Ph-NTs}$ than its phenyl-free 1D tubular counterpart, especially for stability in ethanolysis. Therefore, $\text{ArSO}_3\text{H-Si(Et)Si-Ph-NTs}$ hybrid nanocatalysts show potential for applications in the synthesis of value-added chemicals from biomass-derived platform molecules.

Experimental Section

Materials

Pluronic P123 ($\text{EO}_{20}\text{PO}_{70}\text{EO}_{20}$, $M_w = 5800$), BTMSE (97%), 3-mercaptopropyltrimethoxysilane (MPTMS, 95%), PhTMS (97%), and levulinic acid (98%) were purchased from Sigma-Aldrich. CSPTMS (50% in dichloromethane) was obtained from Gelest Inc. Furfuryl alcohol (98%) was purchased from Sinopharm Chemical Reagent Co. Ltd. Ethyl levulinate (> 98.0%) was purchased from TCI. 2-(Ethoxymethyl)furan (> 95%) was purchased from Bide Pharmatech Ltd. Amberlyst-15 was purchased from Alfa Aesar. The reagents were used without further purification.

Catalyst preparation

$\text{ArSO}_3\text{H-Si(Et)Si-Ph-NTs}$

Typically, P123 (1 g) was dissolved in HCl (1.6 mol L^{-1} , 30.75 g) at RT under stirring. The clear P123 solution was heated to 40°C , and BTMSE (1.2 mL) was added. A BTMSE prehydrolysis time of 45 min was used before the addition of CSPTMS (0.47 mL) and PhTMS (0.1 mL) to the above mixture, and the resultant white suspension was stirred at 40°C for 24 h. The molar ratio of the reactants in the initial preparation system was P123/BTMSE/CSPTMS/PhTMS/HCl/ H_2O 0.0372:1:0.22:0.11:28:348. Subsequently, the suspension was transferred to an autoclave and heated at 100°C with a heating rate of 2°C min^{-1} for 24 h. The resulting white powder was air-dried at 60°C overnight, and then the P123 in the product was removed by washing with boiling ethanol. The final product was obtained after air-drying at 60°C for 12 h, and it is denoted as $x\text{ArSO}_3\text{H-Si(Et)Si-Ph-NTs}$. Herein, x [wt%] is the loading SO_3H groups in the product, which was determined by using an ICAP6300-Thermoscientific ICP-OES. The $\text{ArSO}_3\text{H-Si(Et)Si-Ph-NTs}$ materials with different x values were obtained by adjusting the amount of CSPTMS added.

$\text{ArSO}_3\text{H-Si(Et)Si-NTs}$

The procedure is similar to that for the $\text{ArSO}_3\text{H-Si(Et)Si-Ph-NTs}$ hybrid materials, but PhTMS was not used in the preparation system. The molar ratio of the reactants was P123/BTMSE/CSPTMS/HCl/ H_2O 0.0372:1:0.22:28:348.

$\text{PrSO}_3\text{H-Si(Et)Si-NTs}$

The procedure is similar to that for the $\text{ArSO}_3\text{H-Si(Et)Si-NTs}$ hybrid materials, but CSPTMS was replaced by MPTMS (1 mmol) to provide PrSO_3H groups in the presence of H_2O_2 solution (30 wt%). The molar ratio of the reactants was P123/BTMSE/MPTMS/ H_2O_2 /HCl/ H_2O 0.0372:1:0.22:1:28:348.

$\text{PrSO}_3\text{H-SBA-15}$

The procedure is similar to that for the $\text{PrSO}_3\text{H-Si(Et)Si-NTs}$ hybrid materials, however, BTMSE was replaced by TEOS (9.25 mmol) to provide a silica framework in the product. The molar ratio of the reactants was P123/TEOS/MPTMS/ H_2O_2 /HCl/ H_2O 0.0372:2:0.22:1:28:348.

Catalyst characterization

TEM was performed by using a JEM-2100F high resolution transmission electron microscope at an accelerating voltage of 200 kV. N_2 porosimetry measurements were performed by using a Micromeritics ASAP 2020M surface area and porosity analyzer after the samples were outgassed under vacuum at 363 K for 1 h and 373 K for 4 h. The surface areas were calculated using the BET equation, the pore size distribution curves were calculated using the BJH desorption branch of the isotherms, and the pore volume was accumulated up to $P/P_0 = 0.99$. Water vapor adsorption isotherms were measured at 298 K with an increase in the pressure by using an automated gas sorption analyzer (Quantachrome Autosorb-iQ). The sample was dried under a dynamic vacuum at 373 K overnight. Before the measurement, the sample was dried again by using the outgas function of the surface area analyzer for 12 h at 393 K. For the measurement of water adsorption, 50 mg sample was used. ^{29}Si MAS and ^{13}C CP-MAS NMR spectra were recorded by using a Bruker AVANCE III 400 WB spectrometer equipped with a 4 mm standard-bore CP-MAS probe head. The dried and finely powdered samples were packed in the ZrO_2 rotor and closed with a Ke-F cap, which was spun at 12 kHz. Chemical shifts for the ^{29}Si MAS and ^{13}C CP-MAS NMR spectra were referenced to the signal of 3-(trimethylsilyl)-1-propanesulfonic acid sodium salt standard ($\delta = 0.0$ ppm) and $\text{C}_{10}\text{H}_{16}$ standard ($\delta_{\text{CH}_2} = 38.5$ ppm), respectively. The sulfur content or SO_3H loading level in the as-prepared hybrid materials was determined by using an ICAP6300-Thermoscientific ICP-OES. Before determination, the samples were dissolved in 2 mol L^{-1} NaOH solution and then diluted with deionized water to suitable volumes. The Brønsted acid site density ($A_{\text{titration}} [\mu\text{eq}(\text{H}^+) \text{g}^{-1}]$) of the as-prepared materials was determined by titration with NaOH solution ($0.0046 \text{ mol L}^{-1}$) according to a method reported previously.^[36]

Catalytic tests

The catalysts were dried for 2 h at 120°C in a vacuum before the catalytic tests.

Esterification of levulinic acid

The esterification of levulinic acid with ethanol was performed in a three-necked round-bottomed glass flask fitted with a water-cooled condenser. The reaction was performed under the conditions of ethanol refluxing temperature, atmospheric pressure, 2 wt% of an air-exposed catalyst, a levulinic acid (9.85 mmol) to ethanol (68.95 mmol) molar ratio of 1:7, and constant volume (5 mL). The concentration of the produced ethyl levulinate was analyzed by using a Shimadzu 2014C GC. The GC was coupled to a flame ionization detector and an HP-INNOWAX capillary column (film thickness, 0.5 μm ; i.d., 0.32 mm; length, 30 m), the operation temperature was 220 $^{\circ}\text{C}$, and the flow rate of nitrogen gas was 1.0 mL min^{-1} . Ethyl laurate was applied as the internal standard. The catalytic activity was evaluated quantitatively from the yield of ethyl levulinate (Y [%]) and TOF [h^{-1}]. Herein, $Y = (M_D/M_T) \times 100$, in which M_D and M_T are the number of moles of ethyl levulinate produced and expected, respectively, and $\text{TOF} = [M_D/(A_{\text{titration}} \times m)] \times t^{-1}$, in which $A_{\text{titration}}$ is the number of equivalents of H^+ in solid acid determined by acid–base titration, m [g] is the mass of the hybrid catalyst used in esterification reaction, and t [h] is the reaction time.

Ethanolysis of furfuryl alcohol

The ethanolysis of furfuryl alcohol was performed in a Teflon-lined autoclave under the conditions of 120 $^{\circ}\text{C}$, furfuryl alcohol (1.15 mmol) to ethanol (69.00 mmol) molar ratio of 1:60 and 1.5 wt% of catalyst, and stirring was applied throughout the reaction. The concentrations of the produced ethyl levulinate and 2-(ethoxymethyl)furan were determined periodically by using a Shimadzu 2014C gas chromatograph fitted with a HP-INNOWAX capillary column and a flame ionization detector. The injection port temperature was 250 $^{\circ}\text{C}$, and the oven temperature was maintained at 60 $^{\circ}\text{C}$ for 5 min and then increased to 180 $^{\circ}\text{C}$ for 10 min at a heating rate of 8 $^{\circ}\text{C} \text{ min}^{-1}$. The GC injector temperatures were 250 $^{\circ}\text{C}$. Ethyl laurate was applied as an internal standard. Similar to the above esterification reaction, the catalytic activity of all catalysts was also evaluated quantitatively from the yield of ethyl levulinate (Y) and the TOF. The intermediates produced during the catalytic processes were identified by GC–MS (HP6890GC–5973 MSD).

Acknowledgements

This work is supported by the Natural Science Fund Council of China (21173036; 21573038; 21573039; 51008056).

Keywords: biomass • heterogeneous catalysis • nanotubes • organic–inorganic hybrid composites • sol–gel processes

- [1] G. W. Huber, S. Iborra, A. Corma, *Chem. Rev.* **2006**, *106*, 4044–4098.
- [2] S. N. Naik, V. V. Goud, P. K. Rout, A. K. Dalai, *Renewable Sustainable Energy Rev.* **2010**, *14*, 578–597.
- [3] M. J. Climent, A. Corma, S. Iborra, *Green Chem.* **2014**, *16*, 516–547.
- [4] D. Ding, J. Xi, J. Wang, X. Liu, G. Lu, Y. Wang, *Green Chem.* **2015**, *17*, 4037–4044.
- [5] R. Mao, Q. Zhao, G. Dima, D. Petraccone, *Catal. Lett.* **2011**, *141*, 271–276.
- [6] Z. H. Zhang, K. Dong, Z. K. Zhao, *ChemSusChem* **2011**, *4*, 112–118.
- [7] A. Démolis, N. Essayem, F. Rataboul, *ACS Sustainable Chem. Eng.* **2014**, *2*, 1338–1352.

- [8] H. Guo, Y. Lian, L. Yan, X. Qi, R. L. Smith, *Green Chem.* **2013**, *15*, 2167–2174.
- [9] K. Jacobson, R. Gopinath, L. C. Meher, A. K. Dalai, *Appl. Catal. B* **2008**, *85*, 86–91.
- [10] X. Duan, Y. Liu, Q. Zhao, X. Wang, S. Li, *RSC Adv.* **2013**, *3*, 13748–13755.
- [11] J. P. Lange, W. D. Graaf, R. J. Haan, *ChemSusChem* **2009**, *2*, 437–441.
- [12] D. R. Fernandes, A. S. Rocha, E. F. Mai, C. J. A. Mota, V. T. Silva, *Appl. Catal. A* **2012**, *425–426*, 199–204.
- [13] P. Carà, R. Ciriminna, N. R. Shiju, G. Rothenberg, M. Pagliaro, *ChemSusChem* **2014**, *7*, 835–840.
- [14] K. Y. Nandiwale, P. S. Niphadkar, S. S. Deshpande, V. V. Bokade, *J. Chem. Technol. Biotechnol.* **2014**, *89*, 1507–1515.
- [15] P. Neves, M. M. Antunes, P. A. Russo, J. P. Abrantes, S. Lima, A. Fernandes, M. Pillinger, S. M. Rocha, M. F. Ribeiro, A. A. Valente, *Green Chem.* **2013**, *15*, 3367–3376.
- [16] J. A. Melero, G. Morales, J. Iglesias, M. Paniagua, B. Hernández, S. Penedo, *Appl. Catal. A* **2013**, *466*, 116–122.
- [17] J. A. Melero, R. Grieken, G. Morales, *Chem. Rev.* **2006**, *106*, 3790–3812.
- [18] F. Su, Y. H. Guo, *Green Chem.* **2014**, *16*, 2934–2957.
- [19] G. Mohammadi Ziarani, A. R. Badiei, M. Azizi, *Sci. Iran.* **2011**, *18*, 453–457.
- [20] T. M. Suzuki, T. Nakamura, E. Sudo, Y. Akimoto, K. Yano, *Microporous Mesoporous Mater.* **2008**, *111*, 350–358.
- [21] B. Lu, S. An, D. Y. Song, F. Su, X. Yang, Y. H. Guo, *Green Chem.* **2015**, *17*, 1767–1778.
- [22] I. K. Mbaraka, D. R. Radu, V. S. Y. Lin, B. H. Shanks, *J. Catal.* **2003**, *219*, 329–336.
- [23] S. Miao, B. H. Shanks, *J. Catal.* **2011**, *279*, 136–143.
- [24] B. Karimi, H. M. Mirzaei, A. Mobaraki, H. Vali, *Catal. Sci. Technol.* **2015**, *5*, 3624–3631.
- [25] X. H. Zhang, F. Su, D. Y. Song, S. An, B. Lu, Y. H. Guo, *Appl. Catal. B* **2015**, *163*, 50–62.
- [26] S. An, D. Y. Song, B. Lu, X. Yang, Y. H. Guo, *Chem. Eur. J.* **2015**, *21*, 10786–10798.
- [27] I. Ogino, Y. Suzuki, S. R. Mukai, *ACS Catal.* **2015**, *5*, 4951–4958.
- [28] D. Y. Song, S. An, Y. N. Sun, Y. H. Guo, *J. Catal.* **2016**, *333*, 184–199.
- [29] E. Serrano, N. Linares, J. Garcia-Martinez, J. R. Berenguer, *ChemCatChem* **2013**, *5*, 844–860.
- [30] A. Bail, V. C. Santos, M. R. Freitas, L. P. Ramos, W. H. Schreiner, G. P. Ricci, K. J. Ciuffi, S. Nakagaki, *Appl. Catal. B* **2013**, *130–131*, 314–324.
- [31] X. Liu, X. B. Li, Z. H. Guan, J. Liu, J. Zhao, Y. Yang, Q. H. Yang, *Chem. Commun.* **2011**, *47*, 8073–8075.
- [32] M. Mandal, M. Kruk, *Chem. Mater.* **2012**, *24*, 123–132.
- [33] L. L. Xu, W. Li, J. L. Hu, K. X. Li, X. Yang, F. Y. Ma, Y. N. Guo, X. D. Yu, Y. H. Guo, *J. Mater. Chem.* **2009**, *19*, 8571–8579.
- [34] S. Subianto, M. K. Mistry, N. R. Choudhury, N. K. Dutta, R. Knott, *ACS Appl. Mater. Interfaces* **2009**, *1*, 1173–1182.
- [35] D. Y. Song, S. An, B. Lu, Y. H. Guo, J. Y. Leng, *Appl. Catal. B* **2015**, *179*, 445–457.
- [36] J. A. Melero, G. D. Stucky, R. Griekena, G. Morales, *J. Mater. Chem.* **2002**, *12*, 1664–1670.
- [37] M. H. Tucker, A. J. Crisci, B. N. Wington, N. Phadke, R. Alamillo, J. P. Zhang, S. L. Scott, J. A. Dumesic, *ACS Catal.* **2012**, *2*, 1865–1876.
- [38] Y. B. Huang, Y. Fu, *Green Chem.* **2013**, *15*, 1095–1111.
- [39] J. A. Melero, J. Iglesias, G. Morales, *Green Chem.* **2009**, *11*, 1285–1308.
- [40] G. M. González Maldonado, R. S. Assary, J. A. Dumesic, L. A. Curtiss, *Energy Environ. Sci.* **2012**, *5*, 8990–8997.
- [41] G. Wang, Z. Zhang, L. Song, *Green Chem.* **2014**, *16*, 1436–1443.
- [42] D. Zuo, J. Lane, D. Culy, M. Schultz, A. Pullar, M. Waxman, *Appl. Catal. B* **2013**, *129*, 342–350.
- [43] K. Nakajima, I. Tomita, M. Hara, S. Hayashi, K. Domen, J. N. Kondo, *Adv. Mater.* **2005**, *17*, 1839–1842.
- [44] I. K. Mbaraka, B. H. Shanks, *J. Catal.* **2005**, *229*, 365–373.
- [45] J. Dacquin, H. E. Cross, D. R. Brown, T. Düren, J. J. Williams, A. F. Lee, K. Wilson, *Green Chem.* **2010**, *12*, 1383–1391.

Received: January 23, 2016

Revised: March 17, 2016

Published online on May 20, 2016